Electronic Supplementary Information for

Enhancing Single-Wall Carbon Nanotube Properties through Controlled Endohedral Filling

Jochen Campo,[1] Yanmei Piao,[2] Stephanie Lam,[1] Christopher M. Stafford,[1] Jason K. Streit,[1] Jeffrey R. Simpson,[2,3] Angela R. Hight Walker[2] and Jeffrey A. Fagan[1,*]

1. National Institute of Standards and Technology, Materials Science and Engineering Division, Gaithersburg, MD USA 20899

2. National Institute of Standards and Technology, Semiconductor and Electronics Division, Gaithersburg, MD USA 20899

3. Towson University, Department of Physics, Astronomy, and Geosciences, Towson, MD 21252

*Corresponding Author: jeffrey.fagan@nist.gov

Certain equipment, instruments or materials are identified in this paper in order to adequately specify the experimental details. Such identification does not imply recommendation by the National Institute of Standards and Technology (NIST) nor does it imply the materials are necessarily the best available for the purpose.

This document reports additional spectroscopic characterization data for organic SWCNT-filling molecules not shown in the main text, photographic demonstration of the effects of filling on resolving solely individualized nanotube populations, data supporting statements of equivalent mass yield in processing to normal methodologies, and data supporting the hypothesis of filler molecule ingestion rather than exterior coverage.

Table of Contents

1. Additional Experimental Detais of Main Contribution

Endohedral encapsulation of filling molecules was performed by adding purified SWCNT powders to a volume of the molecule of interest and incubating them for roughly 24 h with the molecule in its liquid state (in an oven depending on the specific molecule). Pentane, heptane, dodecane, hexadecane, octadecane, eicosane, docosane, tetracosane, tetracontane, *cis*-decalin, *cis/trans* decalin, cyclooctane, 1,2,3,4-hydronaphthalene (Tetralin), perfluoroctane, 1-octadecene, 1-bromohexadecane, 2,2,4,4,6,8,8 heptamethylnonane and mesitylene were purchased from Sigma/Aldrich. Ethyl Acetate was acquired from TayChemCo, octahydroanthracene from Pfaltz & Bauer, Inc., and naphthalene (*purum*) from Fluka. All filler chemicals were used as received.

Bath sonication of some SWCNT/fillant combinations (≈ 5 min) was used to homogenize fibrous (as opposed to powdered) SWCNT soot materials. Post incubation, the mixtures were filtered (Millipore VVLP membrane, 0.1 μm pore size) at room temperature to separate the bulk fillant from the solid nanotubes; ethyl acetate was used to dissolve solid fillants for filtering. The resulting filter cakes (typically 10 – 20 mg) were rinsed with ethyl acetate (as well as aqueous sodium deoxycholate (DOC) solution (20 g/L)) to remove residual bulk fillant, after which they were added to an appropriate volume of 20 g/L DOC/H_2O to achieve a mass loading of ≈ 1 mg/mL SWCNT. In no case was there evidence of nanotube loss in the collected filtrate. The pre-treated SWCNTs were then dispersed as in previous reports through sonication (30 min of tip sonication (6 mm) at ≈ 0.9 W/mL, sample held in an ice water bath) followed by centrifugation for 2 h to remove gross impurities (Beckman JA-20 rotor at 1885 rad/s, retaining the supernatant). Dispersions of SG65i and EG150 SWCNTs (Southwest Nanotechnologies, Norman, OK), P0286 HiPco SWCNTs (Carbon Nanotechnologies Inc.), RN-220 SWCNTs (Raymor Nanotechnologies), P2 electric arc SWCNTs (Carbon Solutions, Riverside, CA), or Tuball SWCNTs (OCSiAl) were prepared separately, generating dispersions with average SWCNT diameters from ≈ 0.8 nm to ≈ 1.7 nm. To ensure accessible cavities for filling of the small diameter nanotubes (CG65i, EG150, HiPco), those populations were bath sonicated in deionized water for 1 h and annealed in a tube furnace under Ar gas at 450 °C for 1 h prior to endohedral filling. To isolate only fully individualized SWCNTs from these dispersions, rate-zonal separation was performed using a Beckman-Coulter L80XP preparative ultracentrifuge (VTi 65.2 (VTi 50) rotor at 6800 rad/s (5240 rad/s) for 0.5 h (3 h) at 20 °C) with a one-step density gradient comprised of a 4 mL race layer containing 12 % – 15 % (mass/volume) iodixanol (sold as OptiPrep, Sigma) and 10 g/L DOC, and a top layer (≈ 0.9 mL) of the SWCNT/fillant dispersion. Post centrifugation, the well-individualized, filled SWCNTs form a band in the mid-upper section of the centrifuge tube (SOI); repeatability was found to be excellent. Stirred ultrafiltration cells (30 kDa or 100 kDa membrane) were

used to remove iodixanol and to exchange H_2O for D_2O from the samples prior to additional characterization.

UV-visible-near infrared (UV-vis-NIR) absorbance spectra were collected on a Cary 5000 UV-vis-NIR spectrometer from 1880 (2500) to 200 nm in H_2O (in D_2O) in 1 nm increments through a (1 or 2) mm quartz cuvette with an integration time of 0.1 s/nm (2 nm bandpass slit width). The spectra of the corresponding blank surfactant solution was collected separately and linearly subtracted during data analysis.

Spontaneous Raman scattering was collected in a collinear 180° backscattering configuration on samples dispersed in DOC with a triple grating spectrometer (Horiba Jobin Yvon T64000) and a liquid nitrogen cooled CCD detector. The reported excitation wavelengths were provided by a HeNe laser (632.8 nm) and a dye laser using Sulforhodamine B (625 to 660 nm) and Rhodamine 110 (575 nm) dyes pumped by an Ar^+ laser (Coherent Innova Sabre with multiline head). In all Raman measurements, approximately 22 mW of power was focused to a spot size <= 100 μm within the liquid sample volume. The integration time per collection (each spectrum was collected 2 X) varied between 10 s and 60 s. Benzonitrile was used as a reference standard to ensure Raman shift accuracy, and its integrated peak intensity at 460.9 cm^{-1} was used to normalize the relative intensities of the Raman spectra at different excitation wavelengths in the contour plots.

NIR fluorescence was measured on a Horiba Jobin Yvon Nanolog-3 spectrofluorometer with a liquid nitrogen cooled InGaAs array detector and a 450 W xenon lamp. Excitation was selected using a dual grating monochromotor with 1200 (grooves /mm) x 500 (blaze, nm) gratings, and a slit selected bandpass of 4 nm. Emission was measured in the right angle geometry with a 5 mm x 5 mm square quartz cuvette through a long-pass filter and dispersed with a 150 x 1200 or 100 x 800 grating onto the array detector. Bandpass for the emission side was set to 4 nm. Integration time at each excitation wavelength were either 20 or 30 s (contour plot). Collected spectra were corrected for the wavelength dependent irradiance of the excitation beam, and the wavelength dependence of the long pass filter and detector train (including grating) was calibrated using a NIST traceable lamp. HiPco populations containing SWCNTs emitting beyond 1300 nm were exchanged into 10 g/L DOC/D_2O solution using ultrafiltration to avoid absorbance of the emitted signal by H_2O.

2. Absorbance Spectra for Additional Filler Molecule Variants

Successful liquid-filling was achieved for all organic molecules attempted with the electric arc (EA) SWCNTs. Due to space limitations and repetitiveness, the spectra of the isolated filler@SWCNT

(utilizing the literature convention to indicate that the molecule is located in the nanotube endohedral volume) absorbance spectra for these dispersions are shown in Figures S1 and S2. For linear alkanes, best results were found (in terms of narrower linewidths and greater peak intensities in the absorbance spectra) for chain lengths of 16 or more carbons; removal of excess alkane became increasingly difficult for chains longer than tetracosane (n = 24) although still achievable. Shorter alkanes, even pentane, generate significant spectral shifts in absorbance, indicating they are ingested by the nanotubes, but generally display broader optical transition line-widths. All alkanes produce shifts significantly greater than ethyl acetate, which was used to rinse off excess alkane (pentane and heptane exposed soots were simply allowed to dry *via* evaporation after filtration as described in the main contribution and were not rinsed with ethyl acetate; excess tetracontane [n = 40] was rinsed off by making use of heptane, in addition to ethyl acetate).

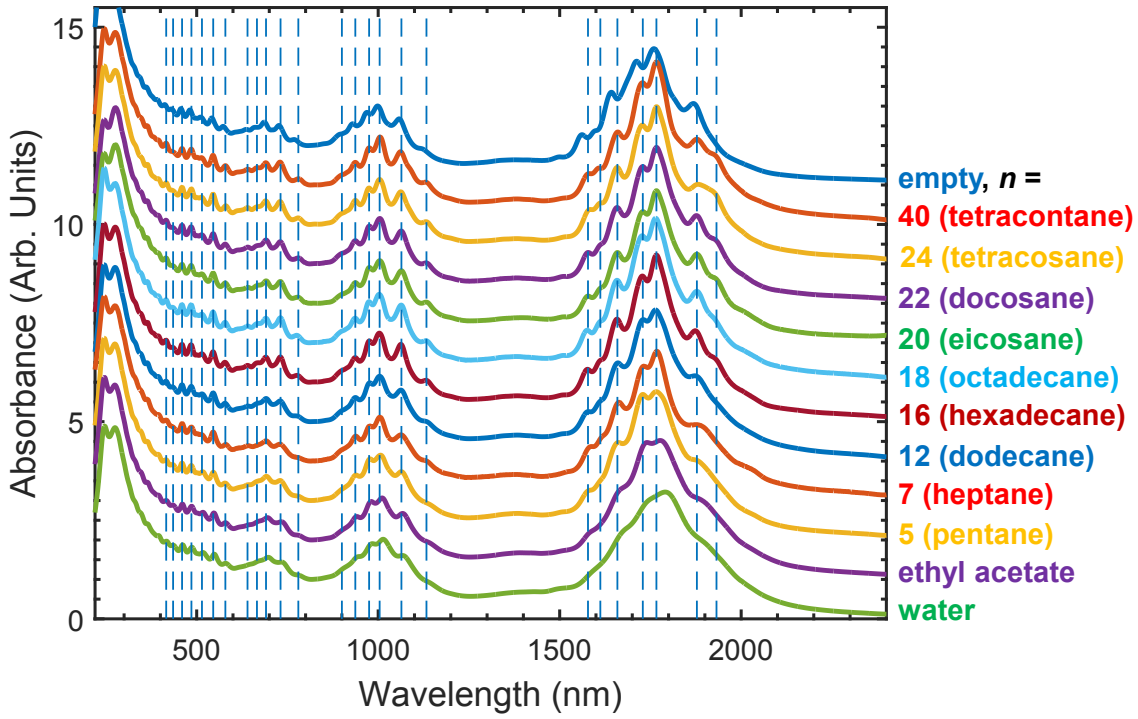

Figure S1. Absorbance spectra of EA SWCNTs filled with linear alkanes (C_nH_{2n+2}) of different lengths compared to empty, ethyl acetate-filled and water-filled SWCNTs (dispersed in aqueous DOC solutions in all cases). The dashed lines indicate the peak positions of the eicosane-filled SWCNTs. The spectra are normalized at their ≈ 810 nm valley and vertically offset with 1 unit.

Many additional organic compounds were used to fill the SWCNTs beyond those shown in the main contribution. Absorbance spectra for the dispersions with these compounds filling the nanotubes are shown in Figure S2. The general effect on the optical transitions is similar on the EA SWCNTs for many of these compounds (all are blue-shifted and sharpened compared to water-filling) and similar to the linear

alkane-filled EA SWCNTs. However, some specific differences in the distribution and locations of certain peak features are observed (in particular for octahydroanthracene) for reasons that probably include packing efficiencies. These differences are beyond the scope of this contribution. The incorporation of these compounds demostrates both the ability to utilize larger molecules as fillants and that additional chemical functionalities can be readily included.

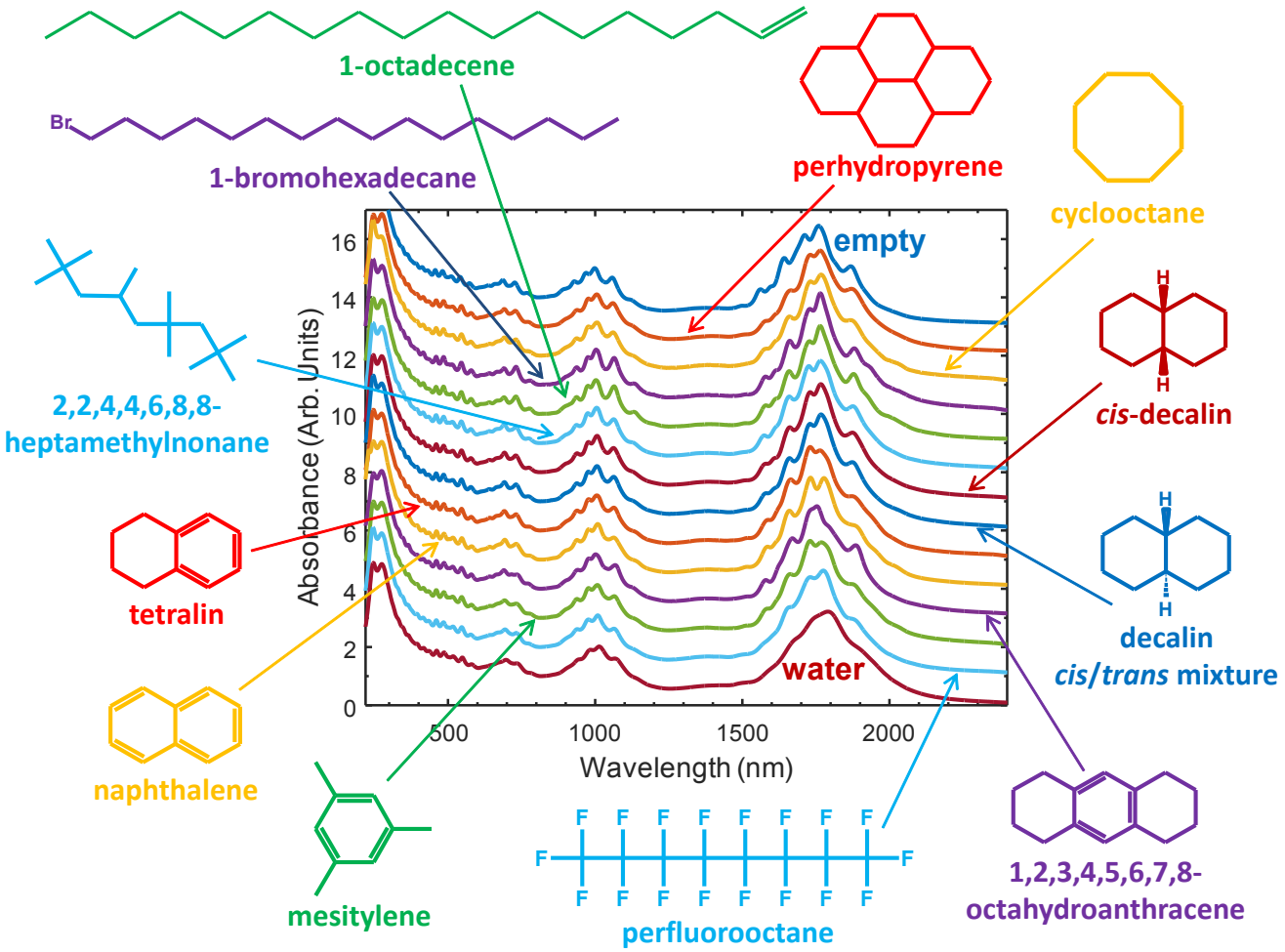

Figure S2. Absorbance spectra of EA SWCNTs filled with various compounds, compared to empty and water-filled SWCNTs (dispersed in aqueous DOC solutions in all cases). The spectra are normalized at their ≈ 810 nm valley and vertically offset with 1 unit. Close inspection reveals that the distribution of absorbance peak features is dependent on the structure of the ingested compound, in particular for the S_{11} transitions, which are most spread out given the wavelength axis scaling.

SWCNTs even larger in diameter than the EA SWCNTs are also readily filled by organic molecules. An example of this is shown in Figure S3, comparing similar diameter water-filled and hexadecane-filled SWCNTs isolated from Tuball SWCNTs. In the hexadecane@SWCNT dispersion the optical transitions continue to be blue-shifted with narrower line-widths as observed for the alkane-filled EA SWCNTs. The broad diameter range of the populations make the peak shifts harder to see, but the

sharpening of the S_{11} transitions is clearly visible. Note that the diameter population is not the same due to the extraction of slightly different layers from the two samples during the rate-zonal processing step discussed below, and is not due to the alkane processing by itself.

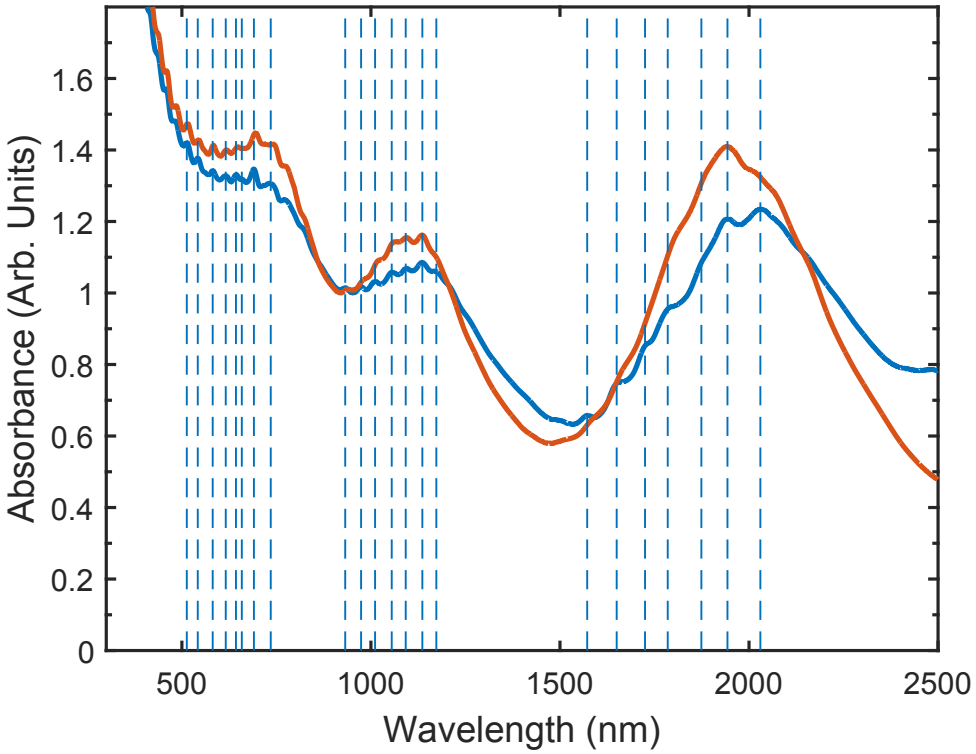

Figure S3. Absorbance spectra of Tuball (OCSiAl) SWCNTs filled with water (red) and hexadecane (blue), dispersed in aqueous DOC solutions. The dashed lines indicate the transition wavelengths of the hexadecane-filled SWCNTs, showing systematic blue shifts and clear line narrowing upon hexadecane filling. Both spectra are normalized at their ≈ 900 nm valley.

3. Mass Yield Statement Support

A motivating reason for this work is the limited mass fraction of empty SWCNTs in a dispersed SWCNT population even from unpurified SWCNT material (the fraction of closed-ended SWCNTs in chemically purified powders is close to zero). One potential benefit of filling the cores of the nanotubes with an organic molecule is that the fraction of empty-like nanotubes could potentially reach 100 %. However, to be useful, the process cannot significantly reduce the general dispersion efficiency or little total gain will be realized. In Figure S4 representative examples of absorbance spectra from sonicated only (in 20 g/L DOC) and sonicated/centrifuged (see Methods) P2 grade EA SWCNTs (light chemical purification) either pre-filled purposely with docosane or allowed to spontaneously fill with water are shown. Mass loadings of the two samples were nominally the same as were the dispersion procedures.

The fractional yield observed is actually greater for the docosane-filled sample in Figure S4, implying that the filling procedure is not detrimental to overall mass yield.

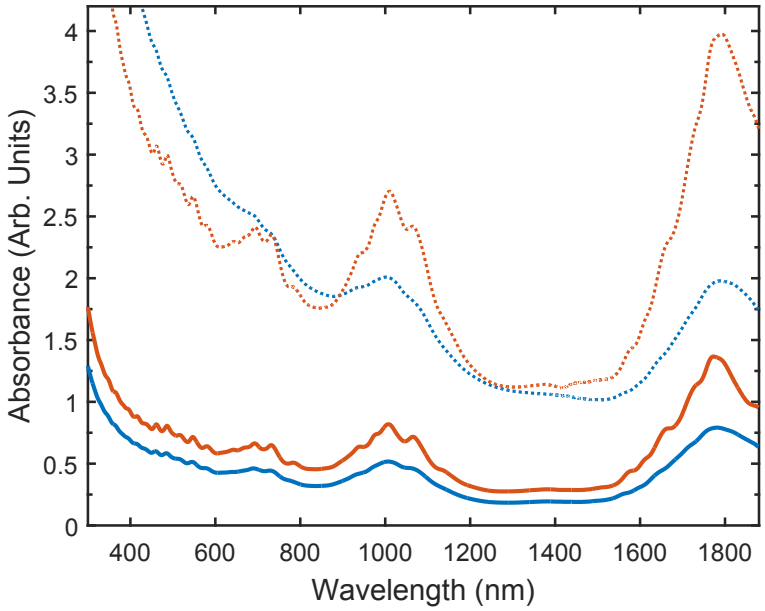

Figure S4. Absorbance spectra (1 mm path length) of water- (blue) and docosane-filled (red) EA SWCNTs, after sonication only (dotted lines), and after centrifugation (2 h JA-20 rotor at 1884 rad/s (18 krpm), solid lines). Both the line narrowing and spectral shifts due to the alkane filling are already visible in these spectra, prior to the more thorough purification by rate-zonal centrifugation. The final mass yield of solubilized docosane-filled SWCNTs is comparable to or even better than for the water-filled SWCNTs. An increased peak to baseline ratio of the alkane-filled material in the sonicated-only sample is a common observation. It is probable that optimization of dispersion conditions could improve the absolute mass yield.

4. Rate-Zonal Isolation of Solely Individualized SWCNTs

Populations characterized in the main contribution were all purified using literature standard sonication/low-speed centrifugation processing, followed by application of an additional rate-zonal centrifugation step. The latter step, described in [1] for the separation of empty from water-filled nanotubes, also functions to remove many other materials, such as small number SWCNT bundles, which sediment at a rate significantly different from the targetted population but which are retained under typical centrifugation conditions in the literature. Colloquially, the various components of the dispersion are forced to race each other through a denser race layer (the addition of the density modifier improves contrast between SWCNTs and bundles and stabilizes the race geometry against Taylor instabilities): undesirable components such as small number bundles and highly bent (defective) SWCNTs run faster than the primary component whereas very small contaminants run more slowly. Typical processing for

these experiments was 0.5 – 1 h at 6800 rad/s (65 krpm) in a Beckman-Coulter VTi 65.2 rotor with ≈ 0.8 mL of sample above a 4 mL layer containing 10 g/L DOC and (10 – 12) % by volume iodixanol. Representative results from the separation are shown in Figure S5 for three different filler materials (yielding different average density effective particles and different amounts of diameter driven variation).

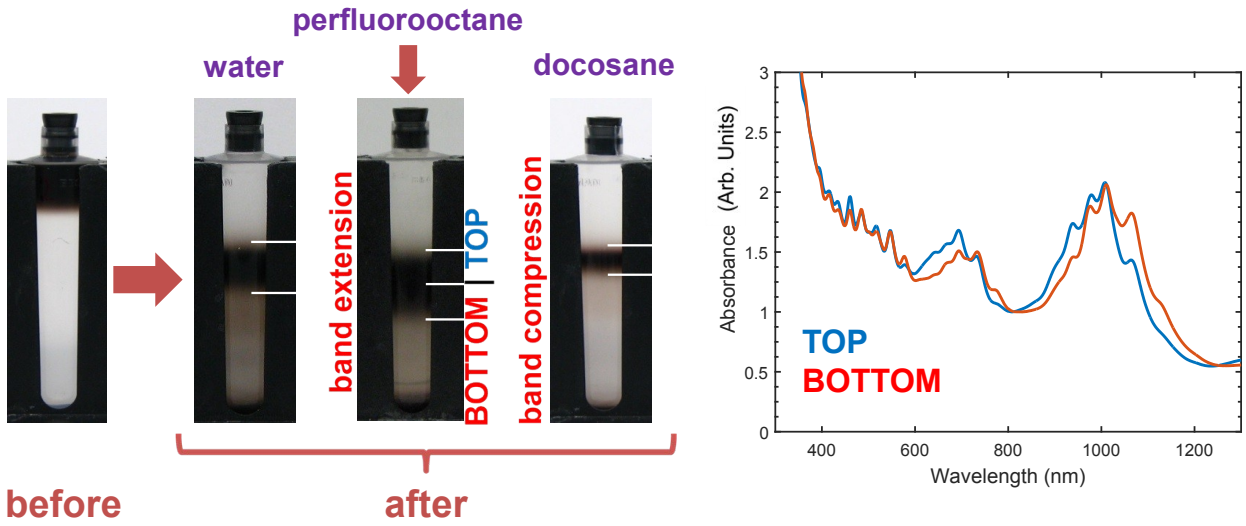

Figure S5. Rate-zonal centrifugation of water- and alkane-filled EA SWCNTs. In agreement with the relative density of the filling molecule, SWCNTs filled with perfluorooctane yield a broader main band (exhibiting a marked diameter dependence; graph on right) compared to water-filled SWCNTs, while docosane-filling on the other hand results in a narrower band. For geometric reasons, the buoyant density of water-filled nanotubes increases with SWCNT diameter; this trend is exacerbated by the incorporation of the high-density perfluoroalkane, and reduced by the ingestion of the alkane.

5. Expanded Scale Absorbance Spectra for Small Diameter SWCNTs

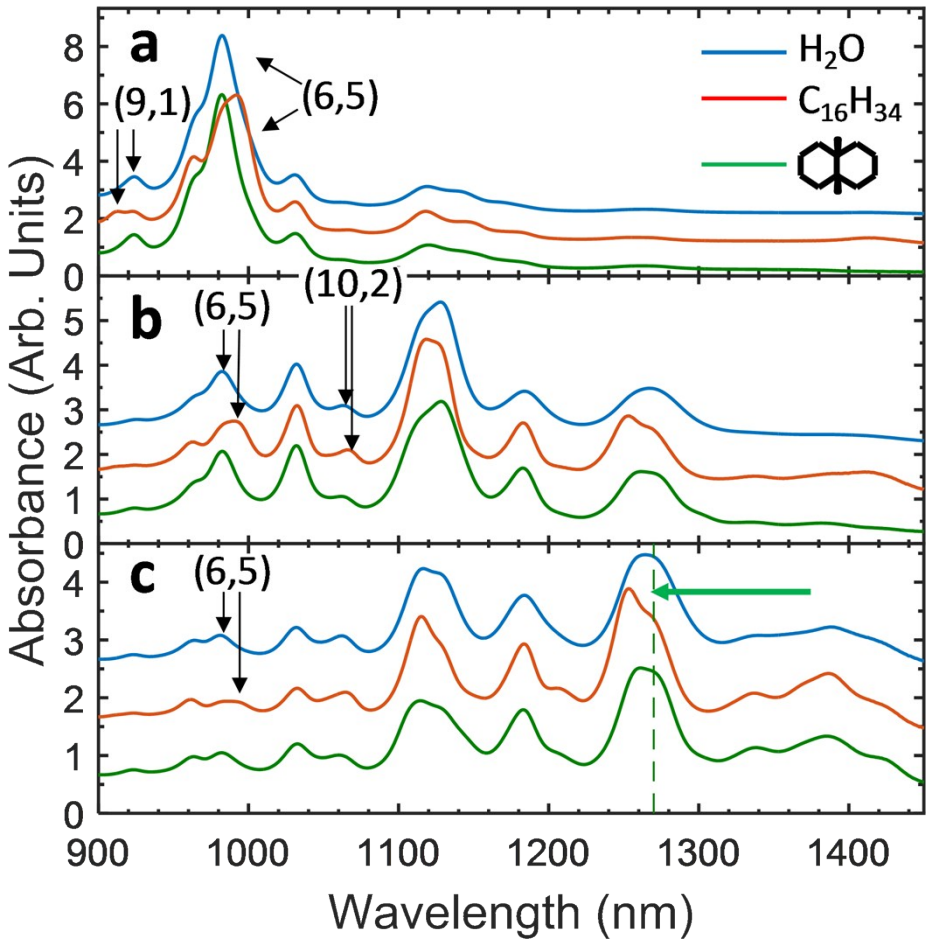

Figure S6. Close-up of Figure 2 of the main contribution: Absorbance spectra of small diameter SWCNTs after purification from (a) CoMoCat SG65i, (b) CoMoCat EG150 and (c) HiPco synthesis methods without controlled filling (blue, water-filled), exposed to hexadecane pre-dispersion (red), and exposed to *cis*-decalin pre-dispersion (green). The dashed line and green arrow indicate the apparent threshold filling diameter for cis-decalin. To aid comparison, spectra were scaled to equal one at the valley between the S_{11} and S_{22} transitions and then vertically offset by 1 unit. Black arrows in each group of spectra highlight the absorbance peak shifts of the (9,1), (6,5) and (10,2) species, demonstrating that alkane filling is present in these nanotubes. Note that the *cis*-decalin is physically too large to be ingested into SWCNTs smaller than a certain diameter (for this molecule those with optical transitions beyond 1250 nm), and thus the green and blue spectra in the 900 nm – 1200 nm range are nearly identical and indicative of water-filled SWCNTs for each population.

6. Additional Experimental Evidence for Ingestion Hypothesis

a. Absorbance Spectra for Alkane-Exposed, Solubilized SWCNTs

The line-narrowing and spectral shifts observed here upon the exposure of SWCNT soot to alkane pre-dispersion are not caused by the previously reported transient micelle swelling for surfactant-coated SWCNTs temporarily exposed to hydrophobic solvents. To demonstrate this, dodecane ($C_{12}H_{26}$) was simply added to a DOC-solubilized water-filled EA SWCNT sample and was stirred for ≈ 24 h. An

aqueous two-phase extraction isolated semiconducting sample was used for this purpose, in order to more clearly see eventual subtle changes in the absorption spectrum. After stirring, the (largely immiscible) aqueous DOC dispersion residing at the bottom was extracted and the absorption spectrum of this sample was compared to the spectrum prior to the alkane exposure (Figure S7). Clearly, both the SWCNT peak positions and line widths are entirely unaffected by this treatment.

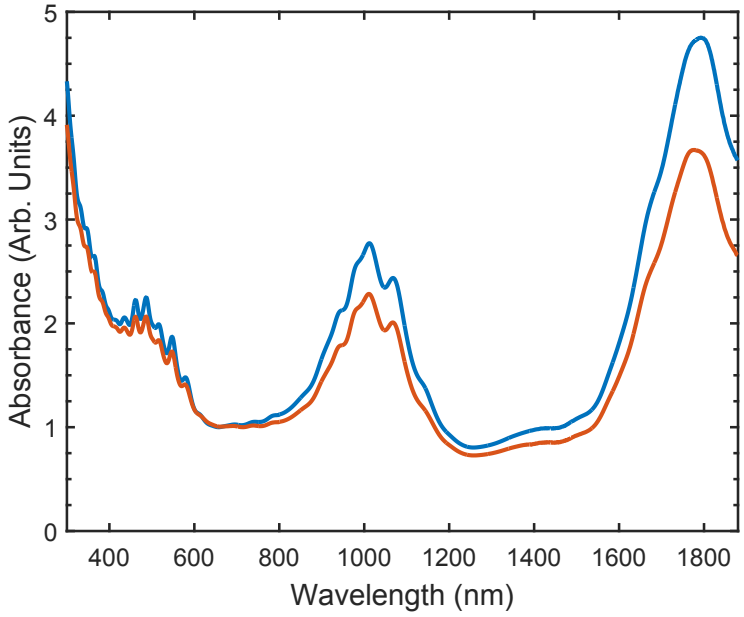

Figure S7. Absorbance spectra of water-filled semiconducting EA SWCNTs in aqueous DOC solutions, unexposed (blue) and exposed (red) to dodecane *after* solubilization. Clearly, the alkane exposure induces no spectral shifts or line-narrowing whatsoever.

b. Absorbance Spectra for Empty (Closed-Ended) Alkane-Exposed SWCNTs

The ingestion hypothesis requires open-ended SWCNTs during the filling step to allow for the ingestion of the filler molecule. For Figure S8, we performed the filling procedure on a raw nanotube powder (non-chemically purified) containing both open-ended and empty (closed-ended) SWCNTs and, following typical dispersion processing, isolated the target populations *via* the rate-zonal methodology. In Figure S8a, empty nanotubes (from raw soot exposed to hexadecane) isolated *via* the rate-zonal separation are compared to empty SWCNTs isolated from water-filled nanotubes (*i.e.*, no alkane exposure). The empty nanotubes from the alkane treated sample do not show any peak shift relative to the empty SWCNTs from the non-alkane treated sample, indicating that the alkane is not adsorbed onto the exterior of the empty nanotubes. As shown in Figure S8b, the exposure of SWCNT soot to alkane only affects the open-ended SWCNTs, resulting in blue-shifts and transition width narrowing as shown in the main contribution. The

diameter difference in the empty and open-ended SWCNT populations is characteristic for the specific SWCNT soot used for this experiment.

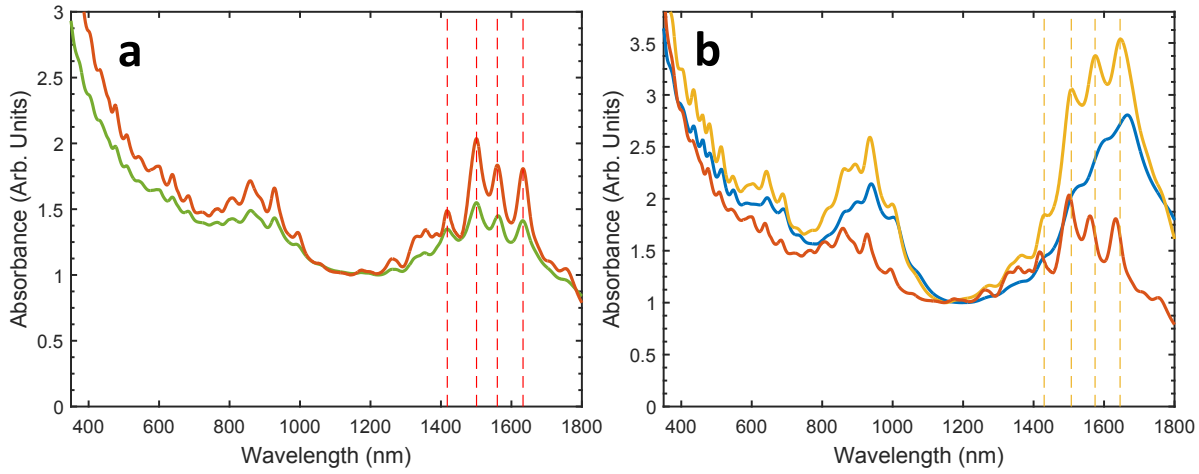

Figure S8. Absorbance spectra of hexadecane-exposed Raymor SWCNTs in aqueous DOC solutions. (a) Closed (empty) SWCNTs exposed (red) and not exposed (green) to hexadecane pre-dispersion. The dashed red lines mark the peak positions of the unexposed empty SWCNTs, which are identical for the primary peaks of the two populations within the experimental uncertainty. The improved peak-to-baseline ratio of the hexadecane-exposed empty SWCNTs is probably due to impurities being rinsed off from the SWCNT soot by hexadecane. (b) Hexadecane-filled SWCNTs (orange), exhibiting the same diameter distribution as the water-filled (blue) and different from the empty (red) SWCNTs. The dashed orange lines mark the peak positions of the hexadecane-filled SWCNTs, clearly blue-shifted relative to the water-filled and red-shifted relative to the empty SWCNTs. All spectra are normalized at the valley between the S_{11} and S_{22} transitions at around 1150 nm.

c. Polarization-Modulation Infrared Reflection-Absorption Spectroscopy (PM-IRRAS) and X-ray Photoelectron Spectroscopy (XPS)

Additional direct evidence for the ingestion of the filler compound into the SWCNTs was pursued through two independent methods using films formed *via* filtration from water-filled and perfluorooctane-filled SWCNTs. SWCNTs filled with a fluorinated compound were chosen for this purpose to enable differentiation of the filler from any of the other chemicals used in the filled SWCNT production sequence. Polarization modulation infrared reflection absorption spectroscopy (PM-IRRAS) and X-ray photoelectron spectroscopy (XPS) were chosen as each has sensitivity for the specific elements present in the sample. In XPS, observation of a fluorine peak is direct evidence that fluorine is unambiguously present in the sample. In PM-IRRAS, differential observation, *i.e.* observation of a signal in one sample and not the other, indicates that the signal is not due to environmental contamination or processing related artifacts.

Briefly, SWCNTs were deposited *via* vacuum filtration from solution onto a Millipore VMWP 0.05 μm pore size membrane followed by an initial rinse of ≈ 100X volume of 9 % ethanol in water, followed by subsequent rinse steps with both water and ethanol.[2,3] The SWCNTs were then transferred to gold-coated substrates as previously reported, with additional rinse steps of acetone, ethanol and water. Films of both the water and perfluorooctane-filled samples were prepared using the same procedure.

For PM-IRRAS, infrared spectra of the thin buckypapers on gold were collected using a Fourier transform infrared spectrometer (Nicolet 6700, Thermo Scientific), equipped with an external polarization modulation infrared absorption spectroscopy (PM-IRRAS) accessory. The accessory includes a photoelastic modulator operating at a frequency of 50 kHz and a half-wave retardation set at 2500 cm^{-1}, a sample holder set at an incident angle of 80°, and a liquid nitrogen cooled mercury-cadmium-telluride (MCT) detector. Spectra were averaged over 100 scans at a resolution of 8 cm^{-1} and baseline corrected using a manual spline function. The samples were also used for compositional analysis *via* XPS, which was performed on a Kratos AXIS Ultra DLD spectrometer with a monochromated Al Kα source operating at 1486.6 eV and 140 W. The base pressure of the sample analysis chamber was ≈ 2.0×10^{-7} Pa. Survey scans were obtained over a binding energy range of (0 to 1200) eV, pass energy of 160 eV, step size of 0.5 eV and dwell time of 0.1 s.

The results of the PM-IRRAS and XPS experiments are shown in Figure S9a and Figure S9b, respectively. In both experiments, peaks attributable to the presence of fluorine are observed solely in the nominally perfluorooctane-filled sample. In PM-IRRAS, we use the differential observation of a peak at ≈ 1240 cm^{-1}, which we can assign to a C-F stretching vibration, in the perfluorooctane-filled SWCNTs that is not present in the unfilled SWCNTs. In XPS, we use the direct observation of the F 1s peak at ≈ 688 eV to explicitly detect the presence of the perfluorooctane within the tubes (C/F ratio ≈ 37.3). Furthermore, the XPS data are consistent with the encapsulation of perfluorooctane, as the measurement was performed at room temperature under high vacuum (10^{-7} Pa) and the vapor pressure of perfluorooctane is ≈ 354 Pa at room temperature.

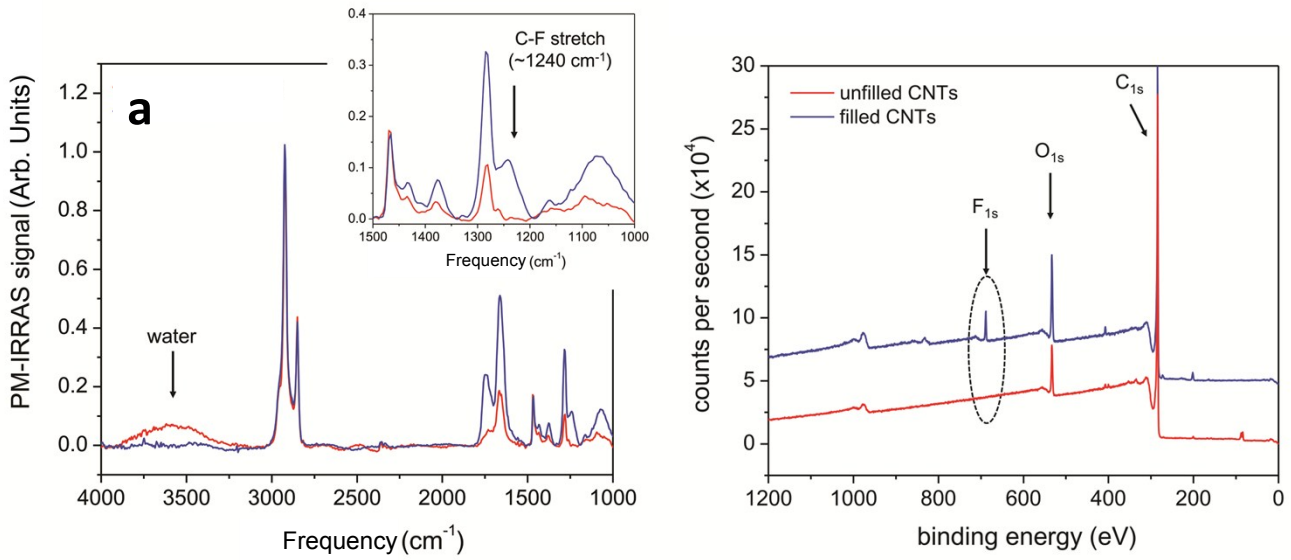

Figure S9. (a) PM-IRRAS and (b) XPS spectra for buckypapers of water-filled (red) and perfluorooctane-filled (blue) EA SWCNTs. The inset in (a) shows a close-up of the C-F stretching vibration at ≈ 1240 cm^{-1}, and the ellipse in (b) indicates the singlet peak associated with F 1s at ≈ 688 eV, both of which are clearly only present for the perfluorooctane-filled sample.

d. Analytical Ultracentrifugation

Analytical ultracentrifugation was performed to establish the densities of the alkane-filled SWCNT complexes. Following published methods,[4,5,6,7] samples of separated water-filled, tetracosane-filled, and perfluorooctane-filled SWCNTs were forcibly dialyzed to remove iodixanol and subsequently diluted into known ratio compositions of H_2O-D_2O or H_2O-iodixanol solutions containing 10 g/L DOC. These samples were then centrifuged in a Beckman-Coulter XLI analytical ultracentrifuge in an AN-50 8 cell rotor with 2-sector epon-charcoal centerpieces at 2617 rad/s (20 krpm) and 20 °C. Data analysis and the theory behind it is described in detail elsewhere.[4-7] Representative sedimentation coefficient (*S*) distributions measured for the three samples, and for the viscosity-corrected sedimentation coefficient as a function of the solution density are shown in Figure S10a and Figure S10b, respectively. The extrapolated intercepts in Figure S10b along the *x*-axis yields the density of the effective particle for the particular experiment; data previously reported for empty nanotubes from the same SWCNT production method are reproduced from reference [7] for comparison.

The anhydrous density (solid lines/symbols in Figure S10b) of an alkane-filled nanotube is expected to be between that of the empty and water-filled SWCNTs based on bulk material densities, and that of a perfluorooctane-filled SWCNT should be greater than the water-filled value. All values measured are consistent with interior cavity filling rather than exohedral coating. For reference, even a thin (0.3 nm)

coating of perfluoroalkane on a water-filled SWCNT (to alternatively account for the improved optical properties) would be expected to yield an anhydrous density of ≈ 1790 kg/m^3 (all else equal).

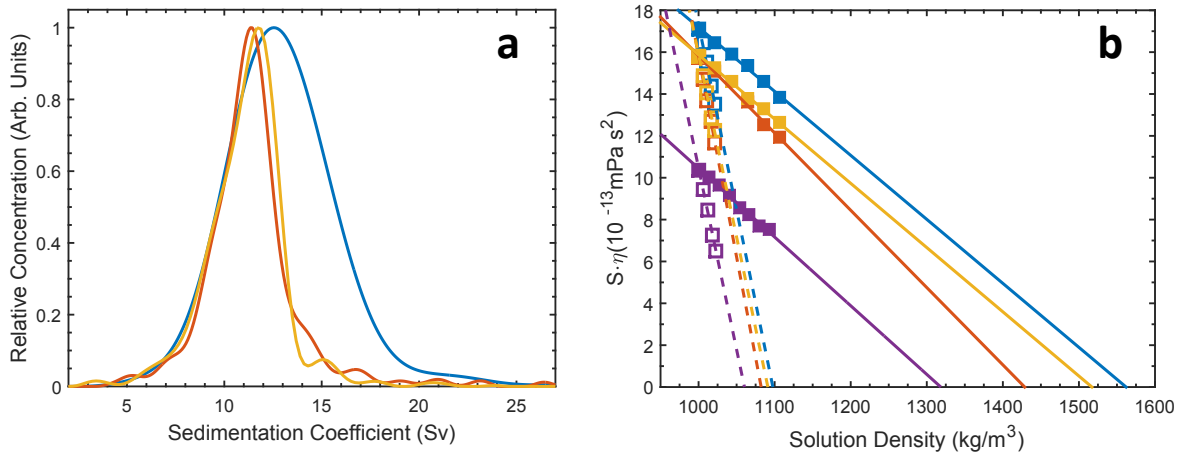

Figure S10. (a) Representative sedimentation coefficient distributions for tetracosane-filled (red), water-filled (orange) and perfluorooctane-filled (blue) EA SWCNTs, as measured in 10g/L DOC/aqueous solution containing 60 % D_2O. The mean sedimentation coefficients are consistent with the relative densities of the filling molecules, and the distribution is strongly broadened for the case of perfluorooctane-filling, caused by the larger density differences between (filled) SWCNTs with different diameters in this case than for water- or tetracosane-filling. (b) Viscosity-corrected mean sedimentation coefficients (symbols) and corresponding linear fits (lines) for empty (dark blue),[7] tetracosane-filled (red), water-filled (orange) and perfluorooctane-filled (blue) EA SWCNTs *vs.* the density of the bulk medium, as adjusted by the amount of D_2O (solid lines, solid symbols) or iodixanol (dashed lines, hollow symbols) present in the aqueous solution at a constant DOC concentration of 10 g/L. The intercepts with the density axis (S = 0) for the D_2O and iodixanol concentration dependent data sets respectively represent the anhydrous and buoyant densities of the corresponding SWCNTs. Error bars in both axes are smaller than the symbols.

e. Additional Resonant Raman Spectroscopy

To further examine the origin of the two RBM peaks observed for the hexadecane-exposed (6,5) species in Figure 3 in the main contribution, their resonance energy profiles were measured (Figure S11). The excitation energy peak positions such obtained for these two peaks indeed reveal a red-shift for the hardened RBM peak, in agreement with the red-shift observed for the S_{22} transition of the hexadecane-filled (6,5) SWCNT relative to that of its water-filled counterpart as derived from absorption and fluorescence-excitation measurements.

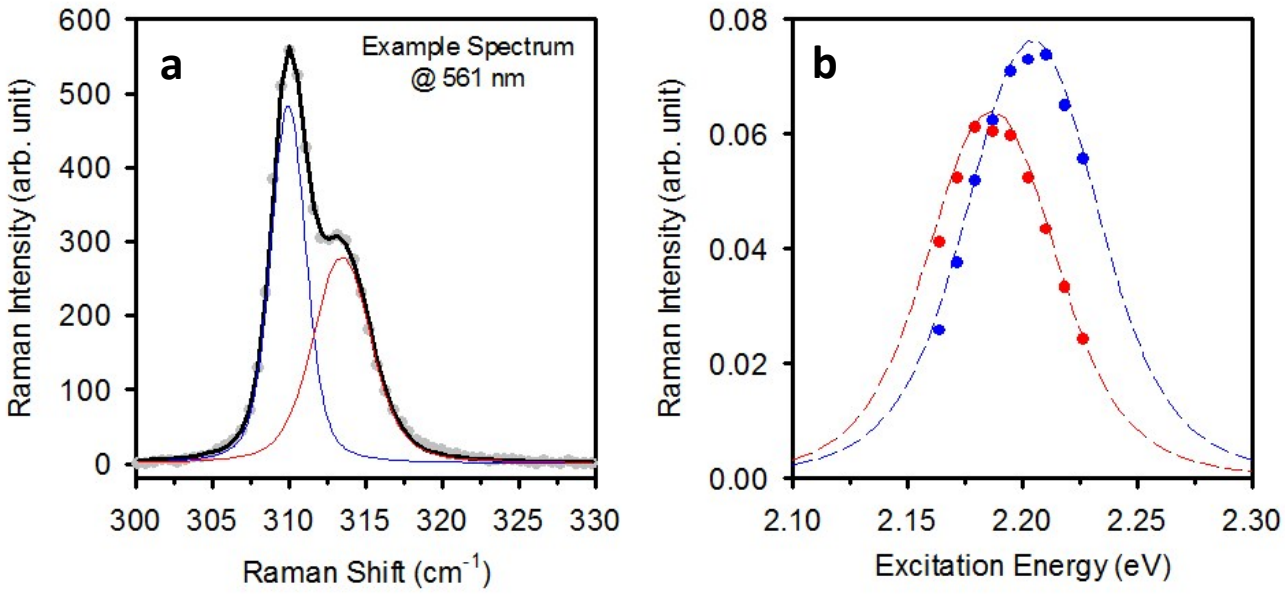

Figure S11. (a) RBM peaks observed for the hexadecane-exposed (6,5) SWCNT in the SG65i CoMoCat sample (excited at 561 nm; grey symbols: experimental data; black curve: fit using two Voigt profiles (red and blue curves)). (b) Raman resonance energy profiles measured for the corresponding RBM peaks depicted in panel (a) (symbols: individual data points; red and blue dashed curves: fit to the data using eq. (1) from reference [8]), clearly showing a red-shift for the hardened RBM peak, which is therefore associated with the hexadecane-filled fraction present in the sample.

Additional Raman data was also collected with other laser excitation wavelengths for the samples shown in Figure 3. Of this data, the primary line of interest for which specific chirality RBMs can be assigned was 632.8 nm. At this line, the (7,6) and (7,5) SWCNT species are near resonance. As seen in Figure S12, in all three SWCNT populations the frequencies of the RBMs for both the (7,5) and (7,6) species are hardened (shifted to higher values) by hexadecane-filling as compared to water-filling.

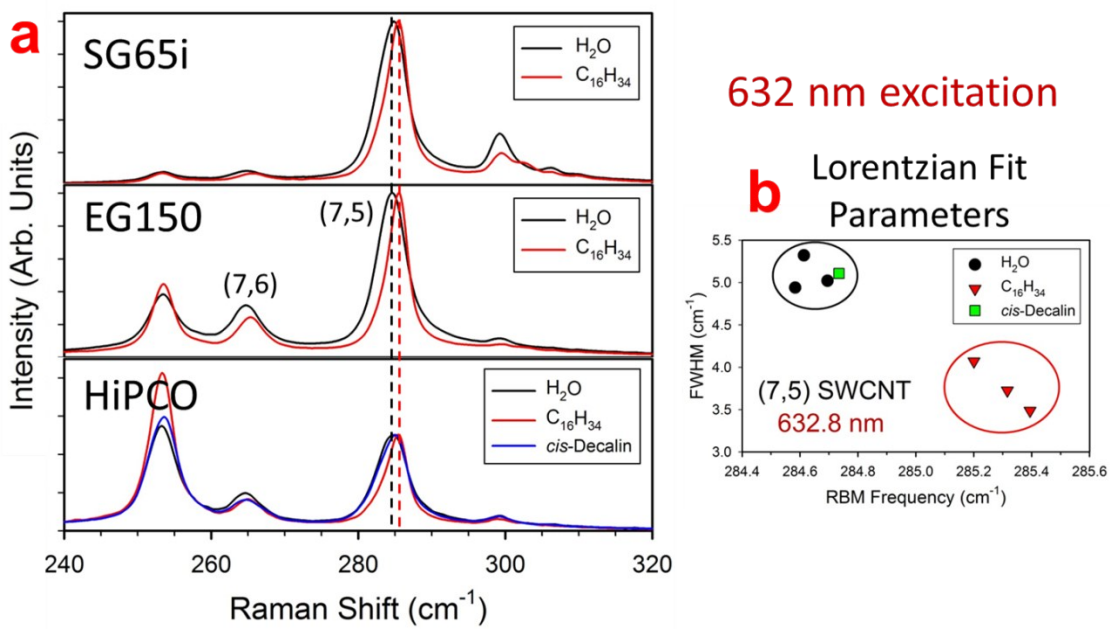

Figure S12. (a) Resonant Raman scattering spectra measured at 632.8 nm excitation for the samples shown in Figure 3 of the main contribution. Hexadecane filling hardens both the (7,6) and (7,5) SWCNT species RBM modes compared to H_2O-filling in a consistent manner across all of the samples. (b) Deconvolution of the spectra using a Lorentzian function for the (7,5) peak feature highlights the similarity of the peak location and width regardless of synthesis method within the separate water and hexadecane-filled groupings. The *cis*-decalin is too large to enter the (7,5) SWCNT, and thus that species is water-filled, with fit peak parameters reflective of the water-filling.

Resonant Raman scattering experiments were also conducted on EA SWCNT samples filled with alkane, water, or that were empty. A comparison of the collected spectra for these samples is shown in Figure S13. Comparing the samples, the greatest observable effect is the change in energy (*i.e.*, *e*xcitation wavelength) of the resonance peak for each SWCNT species (Figure S13a). The peaks of the $C_{18}H_{38}$-filled SWCNTs are red-shifted compared to those of the empty SWCNTs, while they are blue-shifted relative to the water-filled SWCNT peaks, in agreement with absorption (Figure S1). It is additionally clear that, relative to the empty SWCNT sample, the Raman linewidths are broader and the RBM frequencies are hardened for the filled SWCNT samples. A comparison of linescans for the water-filled and a metallic SWCNT-enriched $C_{18}H_{38}$-filled sample indicates slight differences in the degree of hardening or softening of the different RBMs. However, due to the number of SWCNT species present and the difficulty of comparing convolutions of RBMs with (likely) different offsets in resonance energy, no conclusive statements assigning particular values can be made.

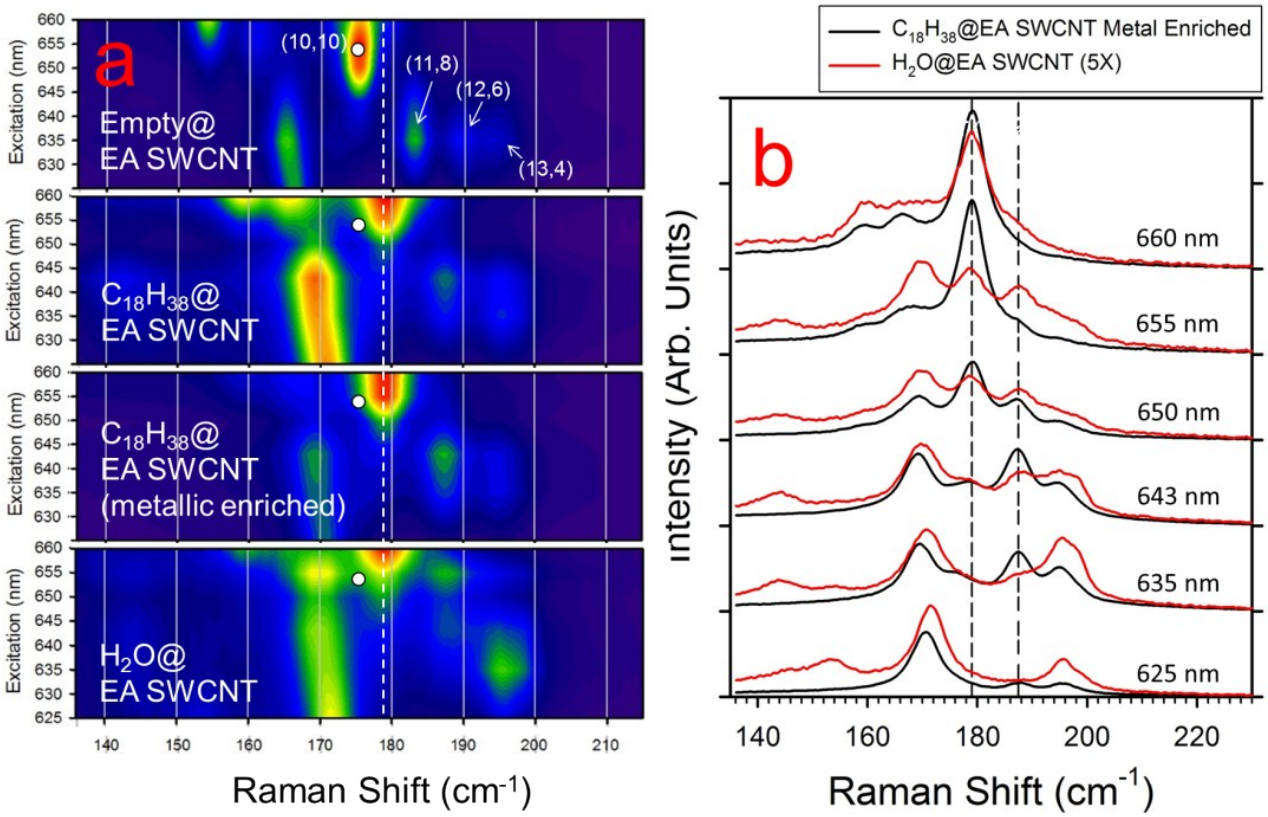

Figure S13. (a) Contour plots of resonant Raman scattering intensity for empty, $C_{18}H_{38}$-filled, $C_{18}H_{38}$-filled and metallic SWCNT enriched, and H_2O-filled EA SWCNTs. RBM assignments are clear for the metallic species in the empty SWCNT sample; the optical transition energy effect on the peak resonance wavelength across the three samples is also clear. The white dots indicate the location of the (10,10) RBM peak in the empty SWCNT sample. (b) Linescan comparison of the RBM shift of the $C_{18}H_{38}$-filled and metallic SWCNT enriched and H_2O-filled EA SWCNT samples at the excitation wavelengths used to construct the contour plots. Differences in the excitation resonance make deconvolution of the spectra for accurate comparison difficult.

f. Additional Fluorescence Spectroscopy

To accurately determine the threshold-size for filling of the narrow diameter SWCNTs with *cis*-decalin, we performed fluorescence-excitation measurements on the *cis*-decalin exposed EG150 SWCNTs, and compared the peak positions and intensities to those for the corresponding water- and hexadecane-filled samples (Figure S14). While the hexadecane-filled sample exhibits a notable increase in fluorescence intensity of all emission peaks (except for the (6,4) tube which is most probably water-filled, see main contribution), the *cis*-decalin sample looks very much like the water-filled sample, as can be expected based on the nearly identical absorption spectrum. Some of the broadest tubes in the population, however (*e.g.*, the (8,6)), clearly exhibit enhanced fluorescence peaks, which are also shifted

in position. This observation, which is most apparent in the integrated fluorescence spectra (Figure S14d), is a sign that these tubes, as opposed to the narrower ones, are actually filled with *cis*-decalin.

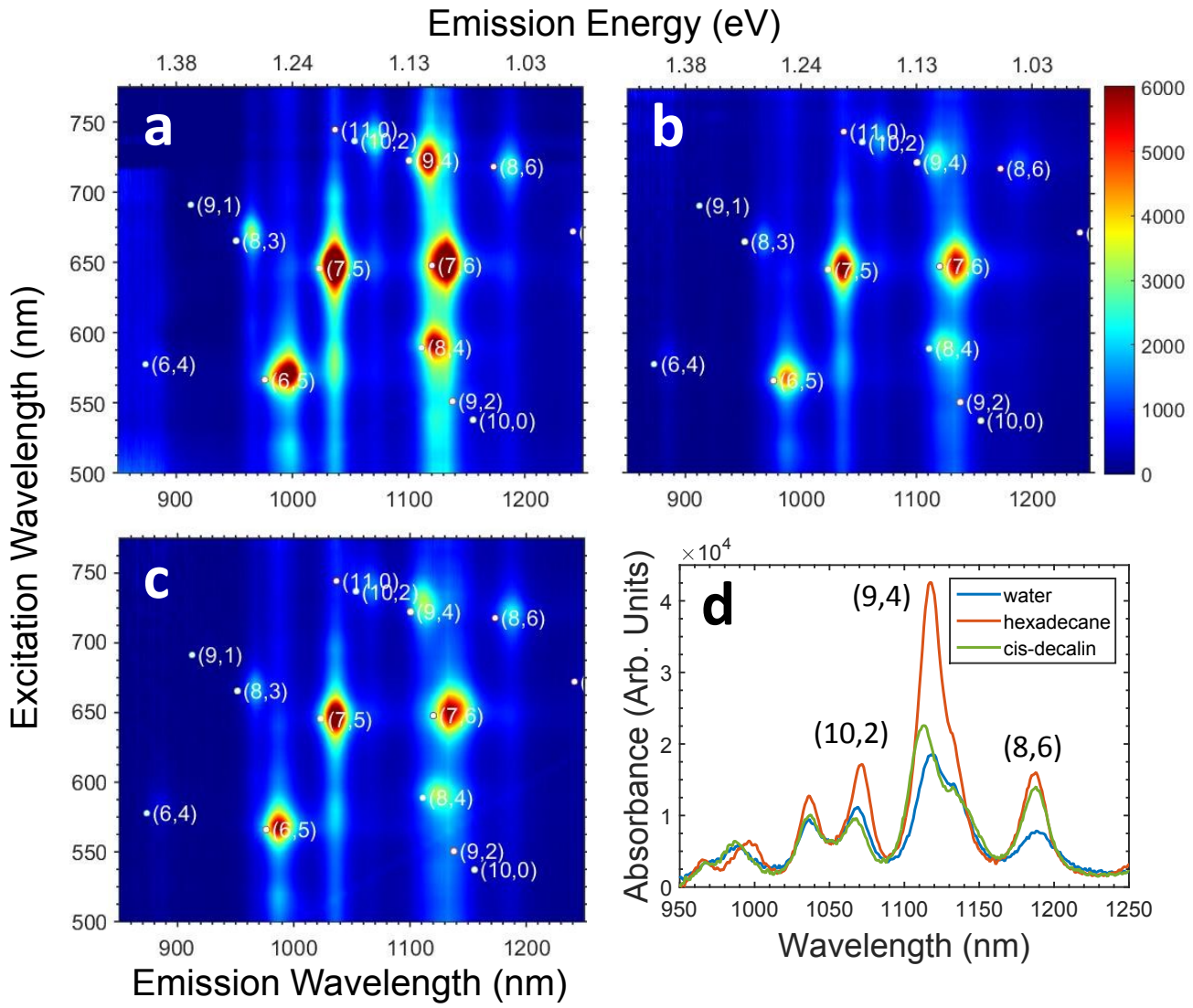

Figure S14. Fluorescence-excitation color maps measured for (a) hexadecane-filled, (b) water-filled and (c) *cis*-decalin treated EG150 CoMoCat SWCNTs, and (d) corresponding integrated emission spectra (λ_{exc} = 705 – 750 nm). All samples were measured at the same concentration (as determined by absorbance) and under identical conditions. All fluorescence maps are plotted using the same intensity scale (see panel (b)). The white dots and labels in the fluorescence maps indicate literature fluorescence peak locations and associated chiral indices for small diameter SWCNT species dispersed in SDS.[9]

7. Perfluorooctane@Polymer Dispersed SWCNTs in Toluene

Demonstration that liquid phase filling of the nanotube cores can be performed for populations to be dispersed in non-aqueous fluids was accomplished utilizing perfluorooctane as the non-soluble filler molecule poly[(9,9-dioctylfluorenyl-2,7-diyl)-alt-co-(6,60-{2,20-bipyridine})] (PFO-BPY) with plasma torch synthesis nanotubes. Similar dispersion efficiency and selection of semiconducting SWCNTs was observed for both the perfluorooctane-filled and toluene-filled SWCNT dispersions. A comparison of the absorbance spectra for the two samples is shown in Figure S15. Although spectral shifts are small compared to the changes observed for the replacement of water by a low-dielectric compound (Figure S1), measurable differences in peak locations are observable in the S_{11} transition region. Packing efficiency differences may be as/more important than dielectric constant contrast.

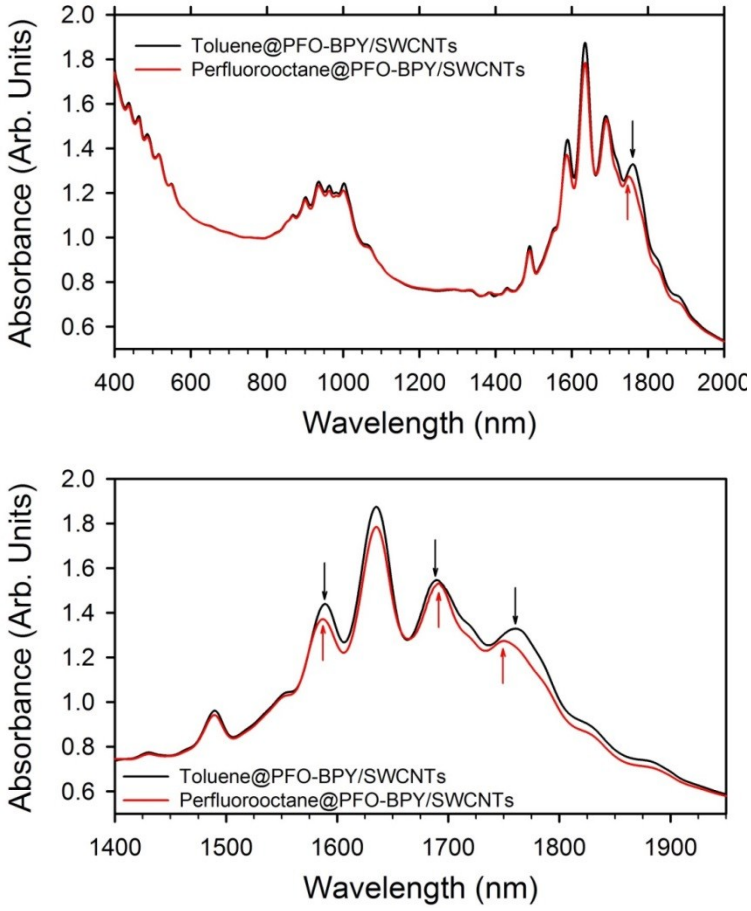

Figure S15. (Top) Absorbance spectra of SWCNTs dispersed in toluene using PFO-BPY polymer, either purposely filled with perfluorooctane, or allowed to advantageously fill with toluene. As expected with PFO-BPY dispersion, a large degree of semiconducting SWCNT species enrichment is observed. (Bottom) Close-up of the 1400 nm to 1950 nm region from above. Differences in peak positions are observed for the dispersed samples with the controlled filling. Vertical arrows highlight the peak shifts in several features.

8. Supplemental References

[1] Fagan, J. A; Huh, J. Y.; Simpson, J. R.; Blackburn, J. L.; Holt, J. M.; Larsen, B. A.; Walker, A. R. H. Separation of Empty and Water-Filled Single-Wall Carbon Nanotubes. *ACS Nano* **2011**, 5, 3943–3953.

[2] Hobbie, E. K.; Simien, D. O.; Fagan, J. A.; Huh, J.; Chung, J. Y.; Hudson, S. D.; Obrzut, J.; Douglas, J. F.; Stafford, C. M. Wrinkling and Strain Softening in Single-Wall Carbon Nanotube Membranes. *Phys. Rev. Lett.* **2010**, 104 (12), 125505.

[3] Harris, J.; Semler, M.; Sylvio, M.; Fagan, J. A.; Hobbie, E. The Nature of Record Efficiency Fluid-Processed Nanotube-Silicon Heterojunctions. *J. Phys. Chem. C* **2015**, 119 (19), 10295–10303.

[4] Schuck, P. Size Distribution Analysis of Macromolecules by Sedimentation Velocity Ultracentrifugation and Lamm Equation Modeling. *Biophys. J. **2000**, 78, 1606-1619.*

[5] Brown, P. H.; Balbo, A.; Zhao, H.; Ebel, C.; Shuck, P. Density Contrast Sedimentation Velocity for the Determination of Protein Partial-Specific Volumes. *Plos One* **2011**, 6, e26221.

[6] Fagan, J. A.; Zheng, M.; Rastogi, V.; Simpson, J. R.; Khripin, C. Y.; Silvera Batista, C. A.; Hight Walker, A. R. Analyzing Surfactant Structures on Length and Chirality Resolved (6,5) Single-Wall Carbon Nanotubes by Analytical Ultracentrifugation. *ACS Nano* **2013**, 7, 3373–3387.

[7] Silvera Batista, C. A.; Khripin, C. Y.; Zheng, M.; Tu, X.; Fagan, J. A. Experimental Validation of Rod Hydrodynamic Scaling with Aspect Ratio using Single-Wall Carbon Nanotubes and Analytical Ultracentrifugation. *Langmuir* **2014**, 30, 4895–4904.

[8] Hároz, E. H.; Duque, J. G.; Barros, E. B.; Telg, H.; Simpson, J. R.; Walker, A. R. H.; Khripin, C. Y.; Fagan, J. A.; Tu, X.; Zheng, M.; Kono, J.; Doorn S. K. Asymmetric excitation profiles in the resonance Raman response of armchair carbon nanotubes. *Phys. Rev. B* **2015**, 91, 205446.

[9] Weisman, R. B.; Bachilo, S. M. Dependence of Optical Transition Energies on Structure for Single-Walled Carbon Nanotubes in Aqueous Suspension: An Empirical Kataura Plot. *Nano Lett.* **2003**, 3, 1235–1238.